PHYSICAL REVIEW C **95**, 051301(R) (2017)

Novel evolution of the positive parity shears band in ^{106}Ag

B. Das,[1] N. Rather,[2] P. Datta,[3,*] S. Chattopadhyay,[2] S. Rajbanshi,[4] A. Goswami,[2] S. Roy,[5] S. Pal,[6] R. Palit,[6] S. Saha,[6] J. Sethi,[6] S. Biswas,[6] P. Singh,[6] and H. C. Jain[6]

[1]*Saha Institute of Nuclear Physics, HBNI, Kolkata-700064, India*
[2]*Saha Institute of Nuclear Physics, Kolkata-700064, India*
[3]*Ananda Mohan College, Kolkata-700009, India*
[4]*Dum Dum Motijheel College, Kolkata-700074, India*
[5]*Manipal Centre for Natural Sciences, Karnataka-576104, India*
[6]*Tata Institute of Fundamental Research, Mumbai-400005, India*

(Received 10 March 2017; published 8 May 2017)

The positive-parity band of ^{106}Ag has been extended up to $I = 25\hbar$ and the lifetimes of the high spin levels of this band have been measured. The deduced transition rates decrease with increasing spin until $I = 21\hbar$. Beyond this spin, the observed transition rates are substantially small and remain nearly constant. This is a novel observation for a shears band. The observed features have been described within the framework of the shears mechanism with a principle axis cranking calculation.

DOI: 10.1103/PhysRevC.95.051301

The shears mechanism was first identified in spherical Pb nuclei in the mass-200 region [1]. These bands are usually characterized by a sequence of strong magnetic-dipole ($M1$) transitions with increasing energies and exhibit a falling trend in their transition rates [$B(M1)$] as a function of spin. The crossover electric-quadrupole ($E2$) transitions are either absent or weak. According to this mechanism, the high-angular-momentum states are generated by the simultaneous closing of the angular-momentum vectors of the valance quasiparticles ($\vec{j}_1$ and $\vec{j}_2$) which are coupled perpendicularly at the bandhead and fully aligned at the highest spin ($\vec{I}_{\rm shear} = \vec{j}_1 + \vec{j}_2$) along the direction of $\vec{I}_{\rm shear}$. It is to be noted that the $\vec{I}_{\rm shear}$ is tilted with respect to the principal axes and the tilt angle remains nearly constant as the band evolves to higher spin states. The shears mechanism has also been observed in moderately deformed nuclei with the suitable single-particle configuration to sustain the shears structure. In these cases, the crossover $E2$ transitions are found to be stronger and the core rotation ($\vec{R}$) also contributes in the generation of angular momentum. As a result, the shears band extends beyond the maximum possible spin $\vec{I}_{\rm shear}$ to $\vec{I}_{\rm max}$, where $\vec{I}_{\rm max} = \vec{I}_{\rm shear} + \vec{R}$ [2]. It is interesting to investigate the fate of a shears band after the blades are completely closed. One possibility is the termination of shears band, which has been proposed in ^{199}Pb [3]. The other possibility is the observation of higher quasiparticle shears structure, which is usually referred to as the crossing of shears bands [4]. However, it is important to note that all the reported shears bands throughout the nuclear chart and irrespective of the core contribution or band crossing exhibit the characteristic falling trend of $B(M1)$ values between bandhead and $I_{\rm max}$ [5].

In the present work, we revisit a previously reported positive-parity shears band in ^{106}Ag and extend it to $I = 25\hbar$. The transition-rate measurements show that the $B(M1)$ transition rates gradually decrease up to $I = 21\hbar$ and then remain nearly constant. This novel feature is investigated in the present work in the context of interplay between core rotation and the shears mechanism.

The high-spin states of ^{106}Ag were populated through the fusion-evaporation reaction ^{96}Zr(^{14}N,4n) using a 68 MeV ^{14}N beam from the Pelletron-LINAC facility at the Tata Institute of Fundamental Research (TIFR), Mumbai, India. An enriched ^{96}Zr of thickness 1 mg/cm^2 with 9-mg/cm^2-thick ^{206}Pb backing was used as the target. The deexciting γ rays were detected by using the Indian National Gamma Array (INGA) [6]. The placement of the detectors along with other experimental details are given in Ref. [7]. The two- and higher-fold coincidence data were recorded in a fast digital data-acquisition system based on Pixie-16 modules of XIA LLC and were sorted in γ-γ matrices and γ-γ-γ cube with a time window of 150 ns by using the sorting program MARCOS [8].

The partial level scheme of the positive-parity band of ^{106}Ag obtained in the present work is shown in Fig. 1. The cube and the symmetric matrix were analyzed by RADWARE programs GTKLEV and GTKESC [9], respectively, to construct this level scheme. The gated spectra projected at 90° were found to be useful to identify the high-spin crossover $E2$ transitions due to the presence of significant Doppler-broadened lineshapes. The sum gate of 258 and 295 keV (Fig. 2) shows the γ rays belonging to this positive-parity band of ^{106}Ag where the newly placed transitions are marked with "$*$." The effect of the Doppler broadening at 90° is clearly visible in the inset of the Fig. 2 for the 1266, 1362, 1424, and 1538 keV transitions, whereas this effect is negligible in the case of the 1495 keV transition, since it is a retarded $E1$ transition. This observation is consistent with the present level scheme and confirms the same reported by He *et al.* [10] until $I^\pi = 21^+$ with few changes.

The previously placed 1212 keV transition between $22^+ \rightarrow 20^+$ is found to be inconsistent because it does not exhibit Doppler broadening whereas the immediately lower $E2$ transition; namely, 1091 keV ($20^+ \rightarrow 18^+$), is Doppler broadened. In addition, the 629 keV ($22^+ \rightarrow 21^+$) transition is not present

*pdatta.ehp@gmail.com

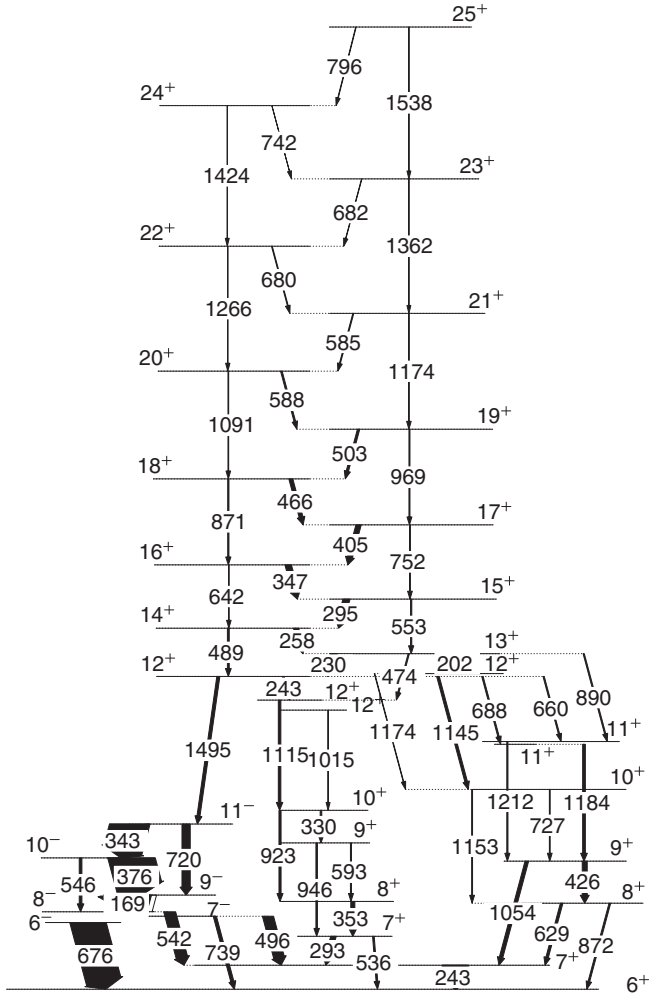

FIG. 1. Partial level scheme of the ^{106}Ag nucleus, where the positive-parity band and its decay path to the ground state has been shown.

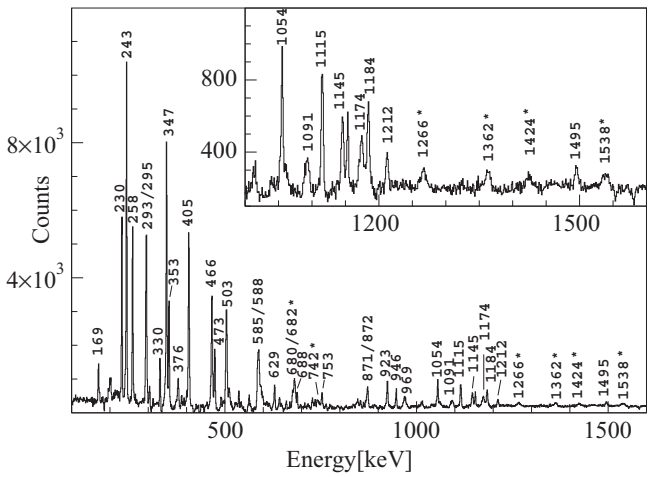

FIG. 2. Sum gated spectra of 258 ($14^+ \rightarrow 13^+$) and 295 ($15^+ \rightarrow 14^+$) keV transitions showing γ transitions belonging to the positive-parity band of ^{106}Ag nucleus. The observed high-energy transitions have been magnified in the inset.

in the sum gate of 1495 and 1145 keV transitions, but two new transitions of 680 and 682 keV are clearly visible. These two transitions have been placed in the present level scheme as the $22^+ \rightarrow 21^+$ and the $23^+ \rightarrow 22^+$ transitions. This placement is further supported by the presence of the two crossover $E2$ transitions, 1266 ($22^+ \rightarrow 20^+$) and 1362 ($23^+ \rightarrow 21^+$) keV, which exhibit the expected Doppler broadening. The level scheme has been further extended to the 25^+ level through the placement of two more $M1$ transitions (742 and 796 keV) and the corresponding crossover $E2$ transitions (1424 and 1538 keV). In the present level scheme, the 629 and the 1212 keV transitions deexcite the lower spin states of 8^+ and 11^+, respectively. These placements are consistent with the gated spectrum shown in Fig. 2. At the lower spin domain, an additional 12^+ level was identified which deexcites to 10^+ through a 1015 keV $E2$ transition. It may be noted that the previously reported [10] $E1$ transition of 1238 keV ($13^+ \rightarrow 12^-$) connecting the negative-parity state could not be confirmed in the present analysis. The spins and parities of the states were firmly established through the directional correlation of oriented nuclei (DCO) and the polarization directional correlation orientation (PDCO) measurements [7] of 1495 ($12^+ \rightarrow 11^-$) and 1145 keV ($12^+ \rightarrow 10^+$) transitions. The values are 0.48(17) and 0.21(13) for 1495 keV and 1.11(15) and 0.35(11) for 1145 keV γ rays, respectively.

The level lifetimes of the high-spin states beyond $I = 16\hbar$ were measured in the present work by fitting the observed lineshapes of the deexciting γ-ray transitions using the code LINESHAPE [11] developed by Wells and Johnson. The details of the code and the general fitting procedure are given in Ref. [7]. The lineshapes were extracted at the specific angles by using the sum gates of 230 and 258 keV transitions on the angle specific matrices. The lifetimes of the 25^+ and 24^+ levels were considered to be effective and then the lower-level lifetimes were measured by using the cascade fit method. The energy levels below $I = 24\hbar$ are fed by two top γ transitions. This effect of the two top level feeds were taken into account through the intensity-weighted average of the half-lives of the feeding levels and was considered as the top-feeding lifetime for the fitting transition. The lineshapes of both the $E2$ and the $M1$ transitions were fit to extract the level lifetimes of the levels with $I < 20\hbar$. The top four $M1$ transitions namely 682 ($23^+ \rightarrow 22^+$), 680 ($22^+ \rightarrow 21^+$), 585 ($21^+ \rightarrow 20^+$), and 588 ($20^+ \rightarrow 19^+$) keV, form two composite lineshapes and cannot be fit by the standard prescription. However, these composite lineshapes have been used to cross-check the level lifetimes which were extracted by fitting the corresponding $E2$ transitions. This was performed by fixing lifetime of one of the levels to the extracted value (e.g., $\tau_{I=23\hbar} = 0.12$ ps) and varying the lifetime of the other ($I = 22\hbar$) to fit the composite lineshape, and vice versa. The other fitting parameters for the levels like side-feeding intensities and quadrupole moments were kept fixed to the values used to fit the corresponding lineshapes of the $E2$ transitions. The four level lifetimes obtained by this procedure agree within $\pm 1\sigma$ with those found by fitting the $E2$ transition lineshapes. This exercise adds to the significance of the reported level lifetimes for $I > 19\hbar$.

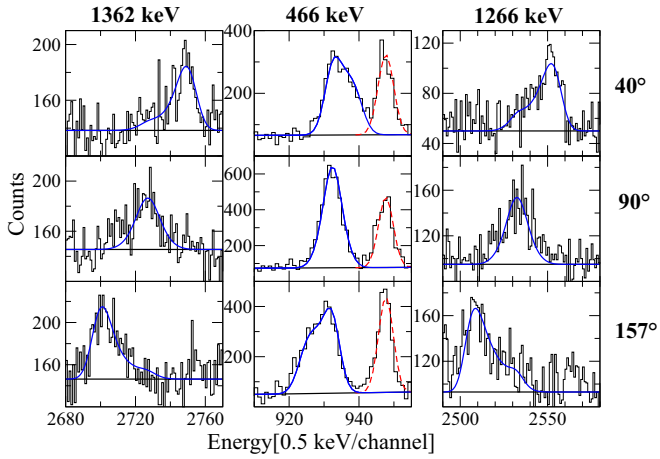

FIG. 3. Examples of lineshape fits for 1362 ($23^+ \rightarrow 21^+$), 466 ($18^+ \rightarrow 17^+$), and 1266 ($22^+ \rightarrow 20^+$) keV transitions at 40°, 90°, and 157° with respect to the beam direction. The calculated lineshapes are shown as solid lines and the contaminant peaks are shown as dashed lines.

To further cross-check the consistency of the level lifetime measurements, the lineshapes of the 466 ($18^+ \rightarrow 17^+$) and 405 ($17^+ \rightarrow 16^+$) keV transitions were extracted from top gating. In these cases, the observed lineshapes were fit by taking into account the complete top cascade but no side feeding at the level of interest. The results from the top and bottom gates were found to agree within $\pm 1\sigma$.

The uncertainties in extracting the level lifetimes were mainly due to the uncertainties of the transition quadrupole moment, the side-feeding quadrupole moment, and the side-feeding intensities. Each of these parameters were varied within the limit of their uncertainties and the corresponding percent errors in the lifetime measurement were added in quadrature to obtain the overall uncertainty. However, this estimate does not include the systematic uncertainty that arises from the choice of the stopping powers. This uncertainty increases from 8% at the low-spin levels to about 15% for the topmost levels. However, it may be noted that this systematic uncertainty is not expected to affect the observed trend in the transition probabilities. The examples of the present lineshape fits are shown in Fig. 3.

The electromagnetic transition rates were deduced from the measured level lifetime for each level. However, it is essential to estimate the mixing ratio δ for the $\Delta I = 1$ transition in order to extract the corresponding $B(M1)$ rates. These were calculated from the measured DCO values by using the program ANGCOR [12] where the value of the width of the substate population (σ/j) was 0.3 [7]. The measured mixing ratios, the $M1$ branching ratios, and the transition rates of the γ transitions are given in Table I and the systematic uncertainty in the extracted lifetime for each level has also been tabulated.

In an earlier work by Deo *et al.* [13], the lifetimes of the $I = 16\hbar$ to $18\hbar$ levels (spin adjusted in accordance with the later publications) were measured by using lineshape analysis with an effective lifetime of 0.31(3) ps for the $I = 19\hbar$ level. The reported values for the $I = 18\hbar$ and $17\hbar$ levels were 0.34(1) and 0.52(2), respectively. These values are in clear disagreement with the present measurement. To investigate this discrepancy, the observed lineshapes from the present work for 466 ($18^+ \rightarrow 17^+$) and 405 ($17^+ \rightarrow 16^+$) keV transitions were fit by assuming an effective lifetime of 0.31(3) ps for the $I = 19\hbar$ level. In this case the extracted lifetimes for the $I = 17\hbar$ and $18\hbar$ levels agree well with the values reported by Deo *et al.* [13]. Conversely, the lineshape for 503 ($19^+ \rightarrow 18^+$) keV transition was fit with a single-level formula and the effective lifetime extracted from the present data was 0.51 ps. The lifetime values for $I = 17\hbar$ and $18\hbar$ extracted with this effective lifetime were found to agree with the results quoted in Table I. Thus, it may be concluded that the discrepancy arose due to an erroneous estimation of the effective lifetime for the $I = 19\hbar$ level by Deo *et al.* [13].

The transition rates from the present work are plotted in Fig. 4. The $B(M1)$ as well as the $B(E2)$ values show a falling trend between the spin range of 17^+ and 21^+ but exhibit near constant behavior afterwards. In the previous works by He *et al.* [10] and Deo *et al.* [13], the origin of this band was attributed to the shears mechanism. This interpretation is consistent with the present analysis up to 21^+. However, beyond this spin the transition rates remain small and nearly constant. This is a novel phenomenon observed in a shears band. It may be noted that the observed $B(E2)$ transition rates of 0.07–0.08 e^2b^2 for the high-spin states are comparable to those for the $2^+ \rightarrow 0^+$ transitions in the near-spherical Sn isotopes [14]. Thus, the

TABLE I. The measured lifetimes, $M1$ mixing ratios, $M1$ branching ratios, the corresponding $B(M1)$ and $B(E2)$ values for the positive-parity band of ^{106}Ag. The statistical errors as well as the systematic errors in lifetime measurement are also tabulated.

Spin [$\hbar$]	Lifetime ±stat. ±sys. [ps]	Mix. ratio ±stat. [δ]	Br. ratio ±stat. [B_r]	$B(M1)$ ±stat. ±sys. [μ_N^2]	$B(E2)$ ±stat. ±sys. [e^2b^2]
17^+	$0.33 \pm 0.04 \pm 0.03$	0.15 ± 0.04	0.80 ± 0.05	$2.03 \pm 0.30 \pm 0.20$	$0.21 \pm 0.03 \pm 0.02$
18^+	$0.21 \pm 0.02 \pm 0.02$	0.18 ± 0.05	0.76 ± 0.05	$1.97 \pm 0.23 \pm 0.23$	$0.19 \pm 0.02 \pm 0.02$
19^+	$0.18 \pm 0.02 \pm 0.01$	0.19 ± 0.06	0.71 ± 0.08	$1.74 \pm 0.28 \pm 0.22$	$0.16 \pm 0.03 \pm 0.02$
20^+	$0.15 \pm 0.03 \pm 0.02$	0.24 ± 0.07	0.55 ± 0.07	$0.97 \pm 0.23 \pm 0.18$	$0.15 \pm 0.04 \pm 0.03$
21^+	$0.22 \pm 0.03 \pm 0.03$	0.21 ± 0.07	0.52 ± 0.06	$0.64 \pm 0.12 \pm 0.11$	$0.08 \pm 0.02 \pm 0.01$
22^+	$0.14 \pm 0.03 \pm 0.02$	0.18 ± 0.07	0.58 ± 0.08	$0.72 \pm 0.18 \pm 0.14$	$0.07 \pm 0.02 \pm 0.01$
23^+	$0.12 \pm 0.02 \pm 0.02$	0.15 ± 0.04	0.48 ± 0.08	$0.70 \pm 0.17 \pm 0.16$	$0.08 \pm 0.02 \pm 0.02$
24^+	0.11	0.15 ± 0.04	0.41 ± 0.08	0.50	0.07

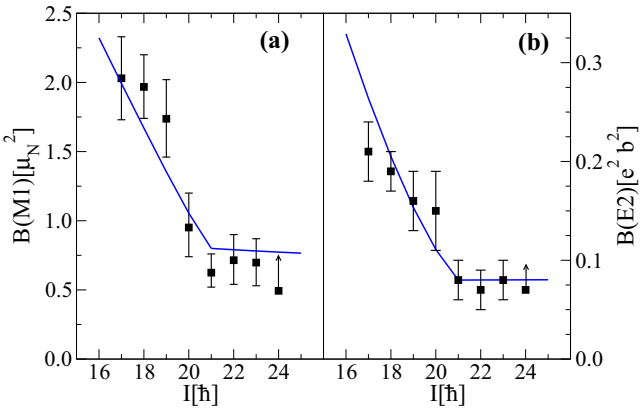

FIG. 4. The measured and calculated (a) $B(M1)$, (b) $B(E2)$ rates for positive-parity band of ^{106}Ag for $\pi g_{9/2}^{-1} \otimes \nu[h_{11/2}^2(g_{7/2}/d_{5/2})]$ configuration. Error bars on measured values of a given level include statistical errors in intensity and the level lifetime added in quadrature. The solid line represents the theoretical values with $\Im = 9\hbar^2/\text{MeV}$ and $V_2 = 1.1$ MeV.

present observation may be interpreted as a transition from the shears mechanism to noncollective rotation.

The most probable single-particle configuration for this positive-parity band is $\pi g_{9/2}^{-1} \otimes \nu[h_{11/2}^2(g_{7/2}/d_{5/2})]$ which has also been proposed in the earlier works [10,13]. For this configuration, the deformation-aligned angular momentum $j_\parallel$ is assumed to be $4.5\hbar$ which corresponds to the proton hole while the rotation-aligned angular momentum $j_\perp = 10.5\hbar$ has been used to reproduce the bandhead spin of $12\hbar$. The maximum angular momentum which can be generated by this shears structure is $15\hbar$. However, the transition rates have been found to decrease steadily up to $21\hbar$, thereby indicating a contribution of $6\hbar$ from the core rotation.

This observation has prompted the use of the shears with the principal axis cranking (SPAC) [15] model, which considers the interplay between shears mechanism and core rotation. In the usual shears model, the core rotation follows the shears angular momentum and the tilt angle θ_I remains fixed [16]. In the present version of the SPAC model, the neutrons stay aligned along the rotation axis due to the Coriolis force, and the shears angle closes solely due to the alignment of the deformation-aligned proton angular momentum [17]. As a result, the tilt angle θ_I decreases with decreasing shear angle θ. This vector coupling scheme is pictorially depicted in Fig. 3 of Ref. [17]. According to this scheme the energy of a state having spin I can be written as [2]

$$E = |\vec{R}(I,\theta)|^2/2\Im + V_2 P_2(\theta), \tag{1}$$

where $|\vec{R}(I,\theta)|$ is the rotational angular momentum, $\Im$ is the effective moment of inertia, and V_2 is the shears energy and the values are determined by fitting the experimental Routhian. The presence of a significant amount of collectivity makes the semidecoupled coupling scheme [2] a good approximation. The contribution of core rotation for every shears angle θ can be estimated from the relation

$$|\vec{R}(I,\theta)| = \sqrt{I^2 - (j_\parallel \sin\theta)^2} - j_\parallel \cos\theta - j_\perp. \tag{2}$$

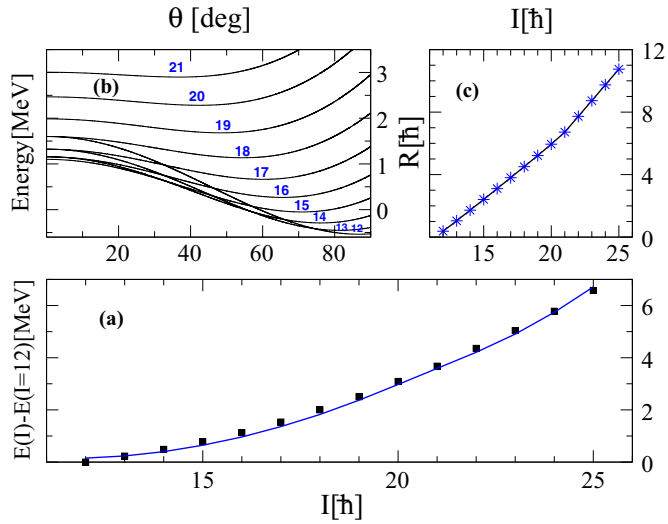

FIG. 5. (a) The measured and the calculated Routhian $[E(I) - E(I = 12)]$, where $E(I = 12)$ is the bandhead energy; and the solid line represents the calculated values from SPAC. (b) The energy minimization plot using SPAC. (c) The core contribution to the total angular momentum as a function of spin.

By using Eqs. (1) and (2), the shears angles are obtained from the energy minimization for every spin state.

In the present calculations, the shears blades are assumed to be maximally closed at $I = 21\hbar$ since the $B(M1)$ values exhibit a falling trend up to this spin. The fit to the Routhian between 12 to $21\hbar$ yields $V_2 = 1.1$ MeV and $\Im = 9\hbar^2/\text{MeV}$, which are consistent with the systematics of this mass region [2,17]. In the present description, the energy levels beyond $I = 21\hbar$ can be generated from the core rotation $[|\vec{R}(I,\theta)|]$ alone while the shears angle θ remains fixed at the minimum value of 36.7°. To obtain the best fit to the observed Routhian, the value of $\Im$ was changed continuously from 9 to $10.5\hbar^2/\text{MeV}$ across $I = 21\hbar$. The calculated Routhian plot and $|\vec{R}(I,\theta)|$ as a function of total angular momentum are shown in Figs. 5(a) (solid line) and 5(c), respectively.

In the framework of SPAC model, the $B(M1)$ values are calculated using the formula [15]

$$B(M1)(I \to I-1) = \frac{3}{8\pi}[j_\parallel g_\parallel^* \sin(\theta - \theta_I) - j_\perp g_\perp^* \sin(\theta_I)]^2, \tag{3}$$

where $g_\parallel^* = g_\parallel - g_R$, $g_\perp^* = g_\perp - g_R$, $g_R = (Z/A)$; $g_\parallel$ and $g_\perp$ are the g factors for the deformation-aligned and the rotation-aligned single particles at the bandhead, respectively; θ_I is the tilt angle, and Z and A are atomic number and mass number of the nucleus, respectively. The $B(M1)$ values were calculated by using the single-particle g-factor values of 1.27 for $g_{9/2}$ protons and 0.21 and -0.21 for $g_{7/2}$ and $h_{11/2}$ neutrons, respectively. The calculated values are shown as solid line in Fig. 4(a). A good agreement between theoretical and experimental $B(M1)$ values can be readily seen from the figure. It is to be noted that, beyond 21^+, the shears angle θ becomes constant; however, θ_I decreases slowly with increasing spin. This accounts for the very slow fall

of the $B(M1)$ rates which is essentially constant within the uncertainties of the present measurement.

Similarly, the $B(E2)$ values can also be calculated within the framework of SPAC model by using the following relation [15]:

$$B(E2)(I \rightarrow I-2) = \frac{15}{128\pi}[eQ_{\rm eff}\sin^2\theta_j + eQ_{\rm coll}\cos^2\theta_I]^2, \quad (4)$$

where $eQ_{\rm eff}$ and $eQ_{\rm coll}$ are the quasiparticle and the collective quadrupole moments, respectively, θ_j is the angle between $\vec{j}_{\parallel}$ and $\vec{J}$ $(= \vec{j}_{\parallel} + \vec{j}_{\perp})$. The values of the quadrupole moments were obtained by fitting the experimental $B(E2)$ values in the spin range of $18\hbar$ to $21\hbar$. For the best fit, we obtain $eQ_{\rm eff} = 4.42\ eb$ and $eQ_{\rm coll} = 0.63\ eb$. The fitted values along with the experimental $B(E2)$ values are shown in Fig. 4(b). The $eQ_{\rm eff}$ is related to the core-polarization effect [2,18] and the present value indicates a polarization charge of $e_{\rm pol} \sim 2e$. This lower value of $e_{\rm pol}$ rules out the possibility of a three-proton-hole configuration for the positive-parity band of ^{106}Ag [17]. The SPAC model predicts a very slow increase in $B(E2)$ rates beyond $I = 21\hbar$ which again is essentially constant within the uncertainties of the present measurement. In the above treatment, the observed phenomena have been described by assuming the complete closure of the shear at $I = 21\hbar$ and then the higher-spin states originate due to the core rotation alone.

However, it may be noted from Fig. 5(b) that the energy minima are quite soft and, thus, the shears angles for the high-spin states ($I > 21\hbar$) may vary within a certain range. Thus, the observed transition rates with 20%–30% uncertainty may also be described by assuming that the shears angle closes very slowly in the spin domain of $21\hbar$ to $24\hbar$.

The success of the SPAC model in describing both the experimental Routhian and the transition rates allows us to develop a physical picture of the angular-momentum generation mechanism in the positive-parity band of ^{106}Ag. At lower spins, the shears mechanism is predominantly responsible for the generation of the angular momentum with about 30% contribution from the rotation of a deformed core. The shears mechanism reorients the proton angular momentum which leads to the falling trends in the transition rates until $I = 21\hbar$. Beyond this spin, the variation in the shears angle almost vanishes and the transition rates remain nearly constant. Since the electric-quadrupole rates remain small, the possibility of the re-emergence of collective rotation along this band beyond $I > 21\hbar$ is ruled out. The observed small transition rates can be described by the core rotation but with a nearly constant shears angle.

It may be interesting to note that one of the negative-parity bands of ^{106}Ag exhibits the band-crossing behavior of a shears band due to the presence of a small but significant discontinuity in the transition rates at $I = 18\hbar$ [17,19]. In this case, the four-particle-hole configuration of $\pi g_{9/2}^{-3} \otimes \nu h_{11/2}$ changes to $\pi g_{9/2}^{-3} \otimes \nu[h_{11/2}(d_{5/2}/g_{7/2})^2]$, with two additional neutrons aligning to the rotation axis. However, in the present case the six-particle-hole shears structure has not been observed at higher spin. This is probably due to the fact that the lowest available neutron orbitals of both parities are blocked due to the Pauli exclusion principal for the $\pi g_{9/2}^{-1} \otimes \nu[h_{11/2}^2(g_{7/2}/d_{5/2})]$ configuration of the positive-parity band. Thus, the rotationally aligned five-neutron configuration becomes energetically unfavorable as compared to the negative-parity band of ^{106}Ag.

In summary, the level scheme of the positive-parity band of ^{106}Ag has been extended significantly. The lifetimes of the levels of this band were extracted by using the DSAM technique. The deduced $B(M1)$ and $B(E2)$ values decrease with increasing spin up to $I = 21\hbar$ which is the manifestation of shears mechanism. Beyond $I = 21\hbar$, the transition rates remain substantially small and exhibit a slow gradual change. The comparison between the experimental data and the SPAC calculations seems to indicate a novel observation of a transition from the shears mechanism to the noncollective rotation in the positive-parity shears band of ^{106}Ag.

The authors would like to thank the technical staff of TIFR-BARC pelletron facility for its smooth operation throughout the experiment. The help and cooperation of members of the INGA collaboration for setting up the array are acknowledged. This work was partially funded by the Department of Science and Technology, Government of India (No. IR/S2/PF-03/2003-III). In addition, B.D. would also like to thank SINP for research support, and P.D. [Grant No. PSW-058/15-16(ERO)] would like to thank UGC for research support.

[1] G. Baldsiefen *et al.*, Phys. Lett. B **275**, 252 (1992); A. Kuhnert, M. A. Stoyer, J. A. Becker, E. A. Henry, M. J. Brinkman, S. W. Yates, T. F. Wang, J. A. Cizewski, F. S. Stephens, M. A. Deleplanque, R. M. Diamond, A. O. Macchiavelli, J. E. Draper, F. Azaiez, W. H. Kelly, and W. Korten, Phys. Rev. C **46**, 133 (1992); R. M. Clark *et al.*, Phys. Lett. B **440**, 251 (1998).

[2] R. M. Clark and A. O. Macchiavelli, Annu. Rev. Nucl. Part. Sci. **50**, 1 (2000).

[3] H. Hübel *et al.*, Z. Phys. A: Hadrons Nucl. **358**, 237 (1997).

[4] J. R. Cooper *et al.*, Phys. Rev. Lett. **87**, 132503 (2001); P. Agarwal *et al.*, Phys. Rev. C **76**, 024321 (2007); S. Roy *et al.*, *ibid.* **81**, 054311 (2010).

[5] Amita, A. K. Jain, and B. Singh, At. Data Nucl. Data Tables **74**, 283 (2000).

[6] S. Muralithar *et al.*, Nucl. Instrum. Methods Phys. Res., Sect. A **622**, 281 (2010).

[7] N. Rather *et al.*, Phys. Rev. Lett. **112**, 202503 (2014).

[8] R. Palit *et al.*, Nucl. Instrum. Methods Phys. Res., Sect. A **680**, 90 (2012).

[9] D. C. Radford, Nucl. Instrum. Methods Phys. Res., Sect. A **361**, 297 (1995).

[10] C. Y. He *et al.*, Phys. Rev. C **81**, 057301 (2010).

[11] J. C. Wells and N. R. Johnson, Oak Ridge National Laboratory Report No. ORNL-6689 (1991).

[12] E. S. Macias, W. D. Ruhtur, D. C. Camp, and R. G. Lanier, Comput. Phys. Commun. **11**, 75 (1976).

[13] A. Y. Deo *et al.*, Phys. Rev. C **73**, 034313 (2006).

[14] J. M. Allmond *et al.*, Phys. Rev. C **84**, 061303(R) (2011); B. Pritychenko, M. Birch, B. Singh, and M. Horoi, At. Data Nucl. Data Tables **107**, 1 (2016).

[15] E. O. Podsvirova *et al.*, Eur. Phys. J. A **21**, 1 (2004); A. A. Pasternak *et al.*, *ibid.* **23**, 191 (2005); **37**, 279 (2008); A. A. Pasternak, E. O. Lieder, and R. M. Lieder, Acta Phys. Pol. B **40**, 647 (2009); S. Rajbanshi *et al.*, Phys. Rev. C **89**, 014315 (2014).

[16] R. M. Clark *et al.*, Phys. Rev. Lett. **82**, 3220 (1999).

[17] B. Das *et al.*, Phys. Rev. C **93**, 064322 (2016).

[18] A. Bohr and B. R. Mottelson, *Nuclear Structure* (Benjamin, New York, 1969), Vol. I.

[19] E. O. Lieder *et al.*, Phys. Rev. Lett. **112**, 202502 (2014).